Ceramics International 42 (2016) 15881–15888

Contents lists available at ScienceDirect

Ceramics International

journal homepage: www.elsevier.com/locate/ceramint

Highly sensitive acetone sensor based on Eu-doped SnO_2 electrospun nanofibers

Ziqiao Jiang, Rui Zhao, Bolun Sun, Guangdi Nie, He Ji, Junyu Lei, Ce Wang *

Alan G. MacDiarmid Institute, Jilin University, Changchun, 130012 PR China

ARTICLE INFO

Article history:
Received 20 June 2016
Received in revised form
4 July 2016
Accepted 9 July 2016
Available online 12 July 2016

Keywords:
Eu-doped SnO_2
Electrospinning
Nanofibers
Gas sensor
Acetone

ABSTRACT

In this study, a series of undoped and Eu-doped SnO_2 nanofibers were synthesized via a simple electrospinning technique and subsequent calcination treatment. Field-emission scanning electron microscopy (FESEM), transmission electron microscopy (TEM), X-ray diffraction (XRD) and X-ray photoelectron spectroscopy (XPS) were carefully used to characterize the morphologies, structures and chemical compositions of these samples. The results reveal that the as-prepared nanofibers are composed of crystallite grains with an average size of about 10 nm and Eu^{3+} ions are successfully doped into the SnO_2 lattice. Compared with pure SnO_2 nanofibers, Eu-doped SnO_2 nanofibers demonstrate significantly enhanced sensing characteristics (e.g., large response value, short response/recovery time and outstanding selectivity) toward acetone vapor, especially, the optimal sensor based on 2 mol% Eu-doped SnO_2 nanofibers shows the highest response (32.2 for 100 ppm), which is two times higher than that of the pure SnO_2 sensor at an operating temperature of 280 °C. In addition, the sensor exhibits a good sensitivity to acetone in sub-ppm concentrations and the detection limit could extend down to 0.3 ppm, making it a potential candidate for the breath diagnosis of diabetes.

1. Introduction

In recent years, with increasing concerns about environmental safety and human health, the detection of volatile organic compounds (VOCs) has become an urgent task all over the world. An excessive concentration of VOCs may cause air pollution, explosion and even poisoning without timely monitoring and feedback [1]. As a common reagent in industries and labs, acetone has been widely used to purify paraffin, dissolve plastic and dehydrate tissues in pharmaceutics [2]. This volatile compound has anesthetic effects on the central nerve system, and acetone inhalation will cause damage to kidney, liver and pancreas [3]. Furthermore, the acetone level in human breath can serve as a key biomarker for type-1 diabetes. As reported by clinical data, the mean concentration of the exhaled acetone from a healthy individual is 0.3–0.8 ppm, while that from a diabetic patient is found to exceed 1.8 ppm [4,5]. Therefore, it is of great necessity to develop a high-performance acetone sensor for environmental protection and healthcare purposes.

Gas sensors based on semiconducting metal oxides play an important role in the detection of inflammable and toxic gases because of their on-site and real-time gas monitoring [6–9]. SnO_2, a well-known n-type semiconductor with a wide band gap of 3.6 eV, has been proven to be an ideal sensing material to both reducing and oxidizing gases owing to its high response, low cost and nontoxicity [10]. In general, the gas-sensing mechanism of semiconducting oxides lies on the reaction between target molecules and absorbed oxygen species, which is determined by the active sites and defects existing on the surface layer. Hence, morphology and structure are key factors in the gas-sensing process [11,12]. Taking advantages of small size, high density of sensing sites and large specific surface area, one-dimensional (1D) SnO_2 nanostructures with various morphologies have been developed for the acetone-sensing application, including nanorods [13], nanowires [14], nanosheets [15], nanotubes [16] and nanofibers [17]. In terms of the construction of 1D metal-oxide nanostructures, electrospinning is recognized as a convenient method to produce oxide nanofibers which are long in length, exceptionally uniform in diameter and diversified in composition [18]. The large surface-to-volume ratio of electrospun nanofibers can greatly facilitate the conversion of gas recognition into electric signals, resulting in an attractive sensing behavior for fabricating novel gas sensors. Doping with an extrinsic metal ion is another effective way to improve the gas-sensing performance of metal-oxide-semiconductors. Rare earth oxides, such as La_2O_3 [19], Sm_2O_3 [20] and CeO_2 [21], can serve as sensitizers to increase the amount of active centers on the surface of sensing materials due to their fast oxygen ion mobility and excellent catalytic properties. As one of the rare

* Corresponding author.
E-mail address: cwang@jlu.edu.cn (C. Wang).

http://dx.doi.org/10.1016/j.ceramint.2016.07.060
0272-8842/

earth oxides, Eu_2O_3 with good thermal stability and strong surface basicity offers opportunities to improve the acetone-sensing performance of 1D SnO_2 nanomaterials [22]. Most researchers tend to explore the influences of Eu doping on photoluminescence and magnetic properties [23,24]. However, to the best of our knowledge, no attention has yet been focused on the effects of Eu introduction upon the acetone-sensing behavior of SnO_2 nanofibers.

In this work, we adopted a facile electrospinning route followed by calcination to prepare Eu-doped SnO_2 nanofibers. This simple strategy could be extend to the fabrication of similar metal-oxide doped nanofibers using different precursors. For comparison, pristine SnO_2 nanofibers and Eu-doped SnO_2 nanofibers with different Eu doping levels were prepared using the same raw materials under identical conditions. The acetone-sensing properties of obtained nanofibers were investigated in detail. Finally, the sensing mechanism was also discussed in this paper.

2. Experimental

2.1. Chemical reagents

Ethanol and N,N-dimethylformamide (DMF) were purchased from Beijing Chemical Co. Ltd. Tin(II) chloride dihydrate ($SnCl_2 \cdot 2H_2O$), Europium(III) nitrate hexahydrate ($Eu(NO_3)_3 \cdot 6H_2O$) and polyvinylpyrrolidone (PVP, Mw=1,300,000) were acquired from Sinopharm Chemical Reagent Co. Ltd. All the reagents were analytical grade and used as received without any further purification.

2.2. Preparation of pristine and Eu-doped SnO_2 nanofibers

In a typical procedure, 0.4 g $SnCl_2 \cdot 2H_2O$ was dissolved in a solvent mixture of ethanol (4.4 g) and DMF (4.4 g) under magnetic stirring for 30 min. Subsequently, 0.8 g PVP and a suitable amount of $Eu(NO_3)_3 \cdot 6H_2O$ were added into the above-mentioned mixture. After vigorous stirring for 6 h at room temperature, a homogeneous and clear precursor solution was formed. The viscous precursor solution was then transferred into a glass syringe connected to a high-voltage supply. The electrospinning process was conducted in the ambient atmosphere with a relatively low humidity in order to guarantee the sufficient evaporation of the solvent from jet flow. A direct-current voltage (15 kV) was provided between the syringe needle and the aluminum foil collector at a distance of 20 cm. Finally, the electrospun nanofibers were peeled off from the collector and placed in a crucible. Calcination with a defined heating program was performed at 600 °C for 5 h in air to remove the organic component of PVP and crystallize SnO_2. Pristine SnO_2 nanofibers were prepared following the same procedure except the addition of Eu element.

2.3. Fabrication and measurement of gas sensors

The calcined nanofibers were mixed with several drops of deionized water to form a dilute slurry. The slurry was spin-coated onto a ceramic tube on which a pair of gold electrodes was previously printed. A Ni-Cr heating wire was inserted into the tube to form a side-heated gas sensor. Before the first measurement, all the sensors were dried for 2 days at room temperature and then aged at 200 °C for 12 h. Fig. 1 shows the schematic picture of the sensor device along with the measuring electric circuit. V_H is the heating voltage, V_{test} is the total voltage applied to the sensor resistance R_S and load resistance R_L, V_L is the output voltage across R_L. The sensor resistance R_S can be obtained using $R=R_L{}^*(V_{test}-V_L)/V_L$. Gas-sensing properties were measured by CGS-8 intelligent test system (Beijing Elite Tech Co. Ltd., China) under laboratory conditions (25 °C, 60 RH%). Atmospheric air was used as the referenced and dilute gas. The resistance change of sensor devices was recorded when exposure to the target gas at a certain operating temperature. The sensor response is defined as the ratio R_a/R_g, where R_a is the sensor resistance in air, and R_g is the sensor resistance in the presence of test gas [25]. The time taken by the sensor to reach 90% of the final equilibrium response value is defined as the response time in the case of adsorption, or the recovery time in the case of desorption [26].

2.4. Characterization

The morphologies of specimens were observed using field-emission scanning electron microscopy (FESEM, FEI Nova Nano-SEM) and transmission electron microscopy (TEM, Hitachi S-570). X-Ray diffraction (XRD, PANalytical B.V. Empyrean, with a CuKα radiation) was applied to examine the crystal structures. The chemical compositions of samples were analyzed through X-ray photoelectron spectroscopy (XPS, ESCALAB250 using Al as the exciting source).

3. Results and discussion

3.1. Morphological and structural characteristics

Fig. 2(a–d) display the SEM images of Eu-doped SnO_2 nanofibers with different molar ratios (0 mol%, 1 mol%, 2 mol% and 3 mol%) of Eu. It can be observed that the fibrous network structures are well maintained after calcination, and all the fibers are long, continuous and randomly oriented. The high aspect ratio of nanofibers provides effective ways for electron transport during the gas-sensing process. The morphologies of all synthesized samples were further confirmed by TEM. As shown in Fig. 2(a′–d′), the as-synthesized nanofibers are composed of nanocrystals and rough on surface. The rough surface can increase the contact area between the test gas and active sites. Simultaneously, the micro-scaled pores between adjacent nanofibers and nano-scaled pores among agglomerated grains favor the absorption and diffusion of target molecules. According to the statistics given in Fig. 2(a″–d″), the average diameters of pure SnO_2, 1 mol%, 2 mol% and 3 mol% Eu-doped SnO_2 nanofibers are approximately 113, 108, 103 and 100 nm, respectively. Compared to pure SnO_2 nanofibers, the diameters of Eu-doped SnO_2 nanofibers gradually decrease with the increase of Eu content because of the increasing electric charge of precursor solution with totally ionization of $Eu(NO_3)_3$ [27].

XRD patterns are shown in Fig. 3(a) to validate the crystal structures of final products. All the diffraction peaks can be perfectly indexed to the tetragonal rutile structure of SnO_2 (JCPDS No. 41-1445), and no impure phases corresponding to Eu relative compounds are detected. To investigate the effects of Eu doping on the SnO_2 crystal structure, we magnify the (110) and (101) peaks. From the high-resolution image (Fig. 3(b)), it can be clearly seen that the peaks of Eu-doped SnO_2 nanofibers shift slightly to a lower angle compared with those of pure SnO_2 nanofibers, indicating that Eu^{3+} ions are incorporated into the SnO_2 lattice and occupy the tetragonal Sn^{4+} cation sites of rutile SnO_2 [28]. When the doping level is further increased to 3 mol%, the (110) and (101) peaks recover to a high angle again, implying the saturation of Eu^{3+} substitution in the SnO_2 lattice [29]. Moreover, the major diffraction peaks of Eu-doped SnO_2 nanofibers become weak and broaden, suggesting that the Eu dopant can suppress the growth of large SnO_2 crystallites [30]. Table 1 gives the information about the lattice constants of Eu-doped SnO_2 nanofibers obtained from XRD data and crystallite sizes calculated using the Scherrer formula. It is found that the lattice constants (a and c) of SnO_2 increase with

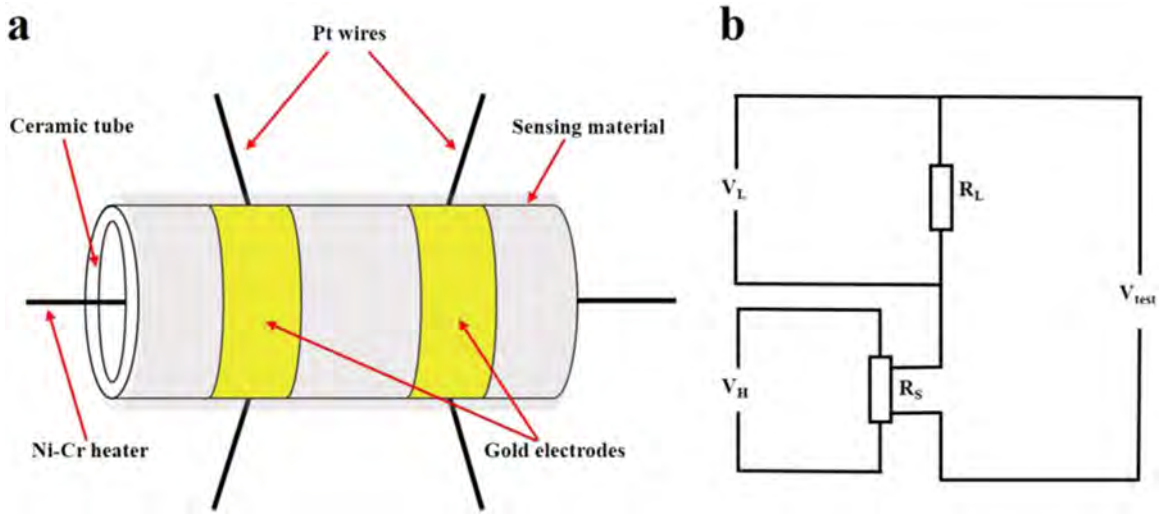

Fig. 1. Schematic picture of (a) the gas sensor and (b) corresponding electric circuit.

increasing Eu concentration. As the ionic radius of Eu^{3+} (0.947 Å) is bigger than that of Sn^{4+} (0.69 Å), the replacement of Sn^{4+} by Eu^{3+} would increase the cell volume. The average crystallite sizes of pure SnO_2, 1 mol%, 2 mol% and 3 mol% Eu-doped SnO_2 nanofibers are 12.0 nm, 11.5 nm, 8.8 nm and 9.8 nm, respectively. The reduction in the crystallite size of SnO_2 by Eu doping allows more active sites on the surface. These results reveal that Eu doping can cause the lattice distortion of SnO_2 and inhibit the growth of SnO_2 crystallites [31].

3.2. XPS analysis

XPS analysis was carried out to illuminate the surface composition and chemical state of the element. Fig. 4(a) shows the XPS survey spectrum of 2 mol% Eu-doped SnO_2 nanofibers, and the energy scale is calibrated with the C 1s peak of adventitious carbon at 284.6 eV. For Sn element (Fig. 4(b)), two symmetric peaks are detected at 486.5 eV and 495.0 eV, which are assigned to $Sn3d_{5/2}$ and Sn $3d_{3/2}$. The energy gap (8.5 eV) between doublet binding energies is in agreement with the standard value [32]. The high-resolution XPS spectrum of Eu 3d is shown in Fig. 4(c). The Eu $3d_{5/2}$ peak centered at 1135.4 eV and Eu $3d_{3/2}$ peak centered at 1165.4 eV is ascribed to Eu^{3+} in Eu_2O_3. The energy difference between two peeks is estimated to be 30.0 eV, which is very closed to the value reported in the standard spectrum of Eu 3d [33]. In contrast to the standard binding energies of Eu $3d_{5/2}$ (1126.0 eV) and Eu $3d_{3/2}$ (1155.0 eV), red shifts of 9.4 eV and 10.4 eV are observed for the binding energies of the Eu $3d_{5/2}$ and Eu $3d_{3/2}$ peaks in Fig. 4(c), respectively. It reveals that the Eu-O distance in Eu-doped SnO_2 is different from that in pure Eu_2O_3 [34]. In other words, the Y-O bond length has changed due to the Eu^{3+} incorporation into the SnO_2 lattice, which is consistent with the XRD result. The inset in Fig. 4(d) is the O 1s spectrum of pure SnO_2. It can be deconvoluted into two gaussian components, a low binding energy (530.8 eV) attributed to the O^{2-} ions (O_L) in the SnO_2 lattice, and a high binding energy (532.0 eV) associated with the O^{2-} ions (O_V) in oxygen-deficient regions within the SnO_2 matrix [35]. However, the O 1s peak of 2 mol% Eu-doped SnO_2 in Fig. 4(d) is asymmetrical with an obvious shoulder. It can be deconvoluted into three gaussian components located at 530.6 eV, 531.7 eV and 532.7 eV, respectively. The two low binding energies are in accordance with those of pure SnO_2, and the highest binding energy at 532.7 eV is originated from the chemisorbed and dissociated oxygen species (O_C) on the surface of Eu-doped SnO_2 nanofibers [36]. The O_C component of pure SnO_2 is not detected, suggesting that Eu doping increases the amount of chemisorbed oxygen. The gas-sensing properties are closely related to the chemisorbed oxygen species [37], thus the high percentage of O_C component (12.81%) implies a high response of Eu-doped SnO_2 nanofibers.

3.3. Acetone-sensing properties

In order to determine the optimal operating temperature for acetone detection, a series of experiments were performed at different temperatures. Fig. 5 presents the dependence of sensor response on the operating temperature. For the pure SnO_2 sensor, the response to 100 ppm acetone increases markedly and reaches its maximum value at the operating temperature of 300 °C, and then decreases with further increasing the operating temperature. A similar trend is observed in the case of the sensors based on Eu-doped SnO_2 nanofibers, and the maximum responses appear at 280 °C. This phenomenon can be explained from the kinetics and thermodynamics of gas adsorption and desorption on the surface of SnO_2. At a low operating temperature, the acetone molecules are not active enough to overcome the activation energy barrier to react with the absorbed oxygen species. When the operating temperature is too high, a few gas molecules may escape away before the reaction due to their risen activation energies [38,39]. Additionally, all Eu-doped SnO_2 nanofibers are more sensitive than pure SnO_2 nanofibers, and the optimal doping ratio of Eu/(Eu+Sn) is 2 mol%. In the following tests, 280 °C was selected as the optimal operating temperature.

The response and recovery behavior is an important parameter to evaluate whether the sensor can rapidly monitor the target molecules in time. Fig. 6(a) depicts the response and recovery characteristics of pure and Eu-doped SnO_2 nanofibers against 100 ppm acetone at 280 °C. The responses of both sensors increase immediately after the test gas is injected, and then recover to the initial baselines sharply when exposure to fresh air. Although the response value of SnO_2 is greatly enhanced by doping Eu, the response and recovery time does not increase. For the 2 mol% Eu-doped SnO_2 acetone sensor, the response and recovery time is about 4 s and 3 s. The rapid response and recovery behavior is attributed to the 1D nanostructure, which can promote the transfer of acetone molecules to the interaction regions and raise the rate for charge carriers to traverse the barrier induced by gas recognition along the fiber [40]. It is also noteworthy that the response and recovery characteristics based on Eu-doped SnO_2 nanofibers are reversible and repeatable, as shown in Fig. 6(b).

To further investigate the sensitivities of fabricated sensors, the

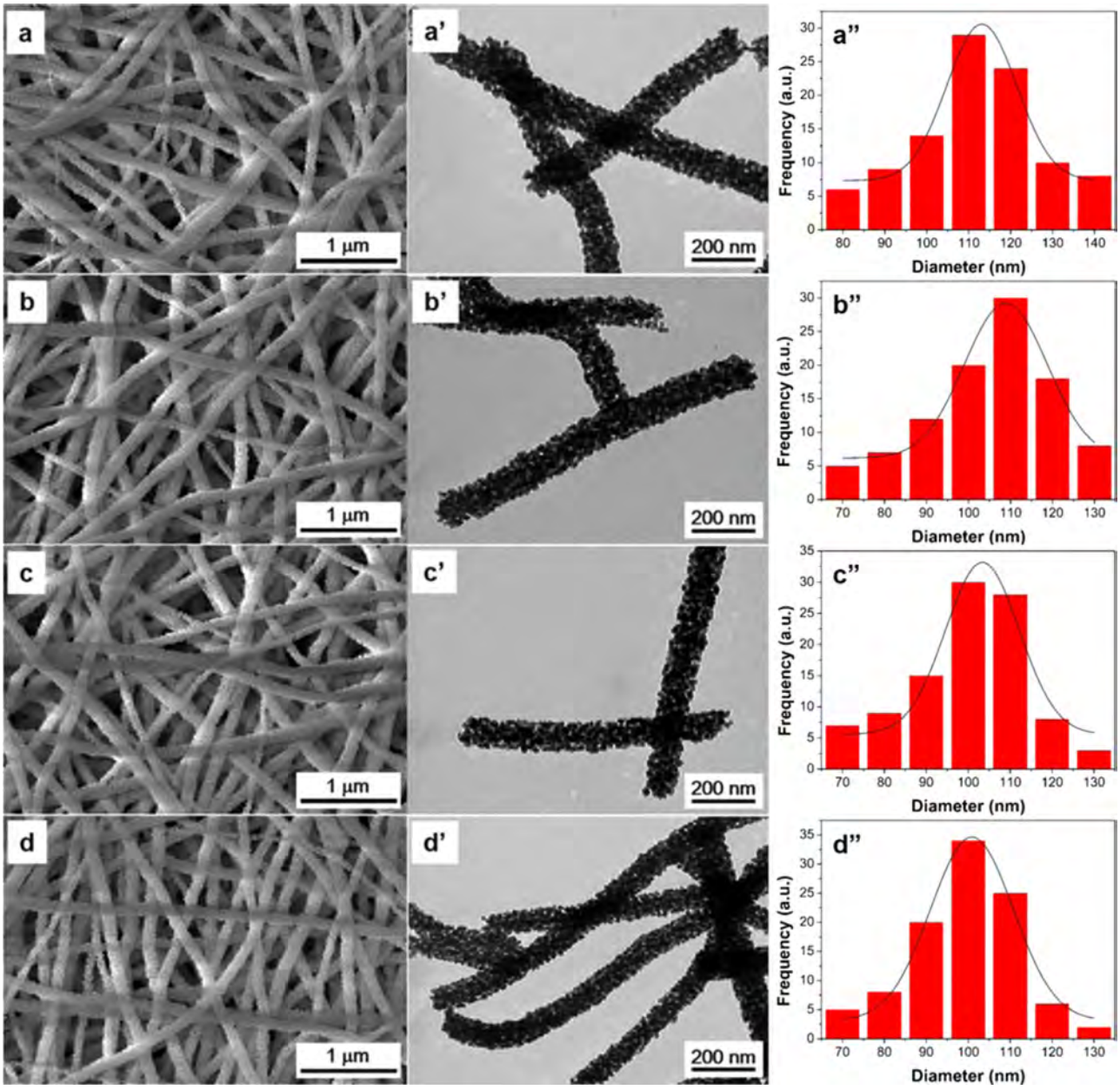

Fig. 2. SEM images, TEM images and diameter distributions of pure SnO_2 nanofibers (a, a′, a″), 1 mol% Eu-doped SnO_2 nanofibers (b, b′, b″), 2 mol% Eu-doped SnO_2 nanofibers (c, c′, c″) and 3 mol% Eu-doped SnO_2 nanofibers (d, d′, d″).

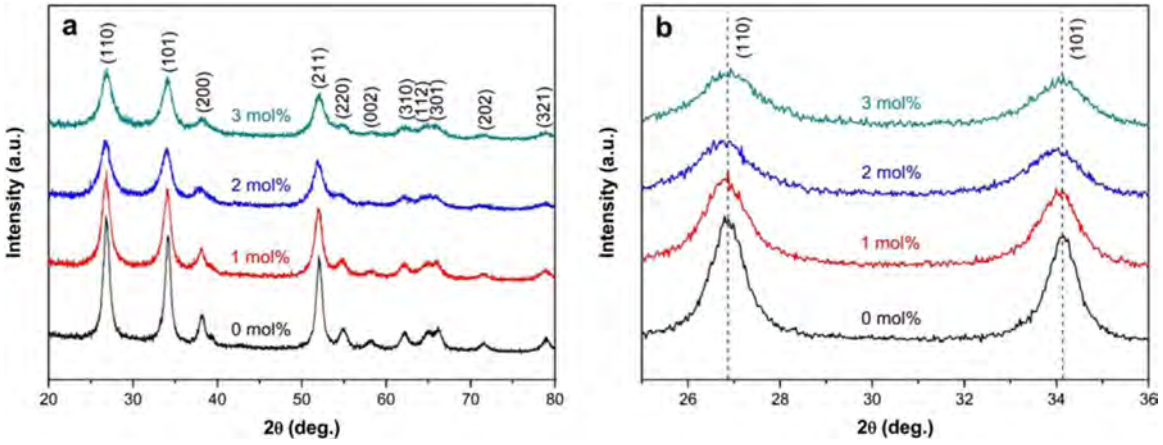

Fig. 3. (a) XRD patterns of pure and Eu-doped SnO_2 nanofibers. (b) high-resolution image of (110) and (101) peaks.

Table 1
A list of the lattice constants, cell volumes and crystallite sizes of pure and Eu-doped SnO_2 nanofibers.

Specimen	Lattice constant a=b (Å)	Lattice constant c (Å)	Cell volume ($Å^3$)	crystallite size (nm)
0 mol%	4.7219	3.1750	70.79	12.0
1 mol%	4.7268	3.1819	71.09	11.5
2 mol%	4.7271	3.1831	71.13	8.8
3 mol%	4.7285	3.1888	71.30	9.8

responses of pure and Eu-doped SnO_2 nanofibers versus different acetone concentrations at the optimal temperature are illustrated in Fig. 7(a). In the range of 10–500 ppm, the responses increase linearly with the increase of acetone concentration. Above 1000 ppm, the increasing rate of response slows down with further increasing acetone concentration, indicating that the sensors become more or less saturated. As for the pure SnO_2 sensor, its response can reach saturation at about 2000 ppm, confirming that no more active sites are available to react with new acetone molecules. However, for the sensors based on Eu-doped SnO_2 nanofibers, the responses are far from fully saturation even increasing acetone concentration up to 5000 ppm, indicating the acetone-sensing enhancement of SnO_2 nanofibers with Eu additive. It is also evident that 2 mol% Eu-doped SnO_2 nanofibers exhibit a much higher sensitivity than pure SnO_2 nanofibers and other Eu-doped SnO_2 nanofibers in the whole detecting range. Fig. 7(b) shows the linear calibration curves in the range of 10–500 ppm. According to the conductance model of semiconducting-oxide sensors, the response can be empirically represented by the following equation [41]:

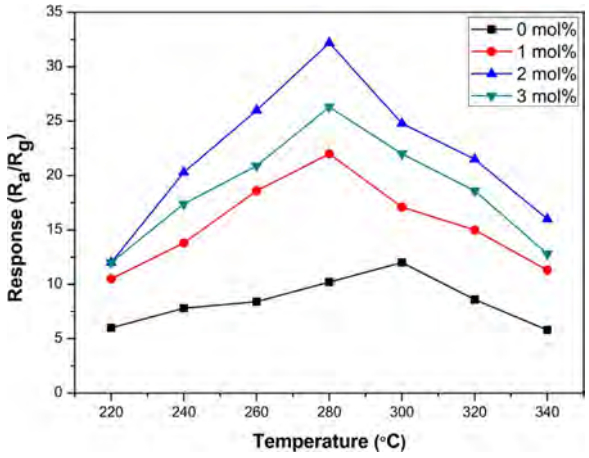

Fig. 5. Responses of pure and Eu-doped SnO_2 nanofibers to 100 ppm acetone as a function of operating temperature.

$$S_g = a\left[C_g\right]^b + 1 \quad (1)$$

where a and b are constants, S_g is the response value, and C_g is the concentration of test gas. The value of b is usually 0.5 or 1, depending on the charge species and stoichiometry of surface reactions. For b is around 0.5, the absorbed oxygen ions are O^{2-}, and for b is around 1, the absorbed oxygen ions are O^- [42]. The b values of both sensors are closer to 0.5, suggesting that the absorbed oxygen ions are mainly O^{2-}. For the detection of trace acetone, the response curve based on 2 mol% Eu-doped SnO_2 nanofibers can be divided into two regions as shown in Fig. 8. It is

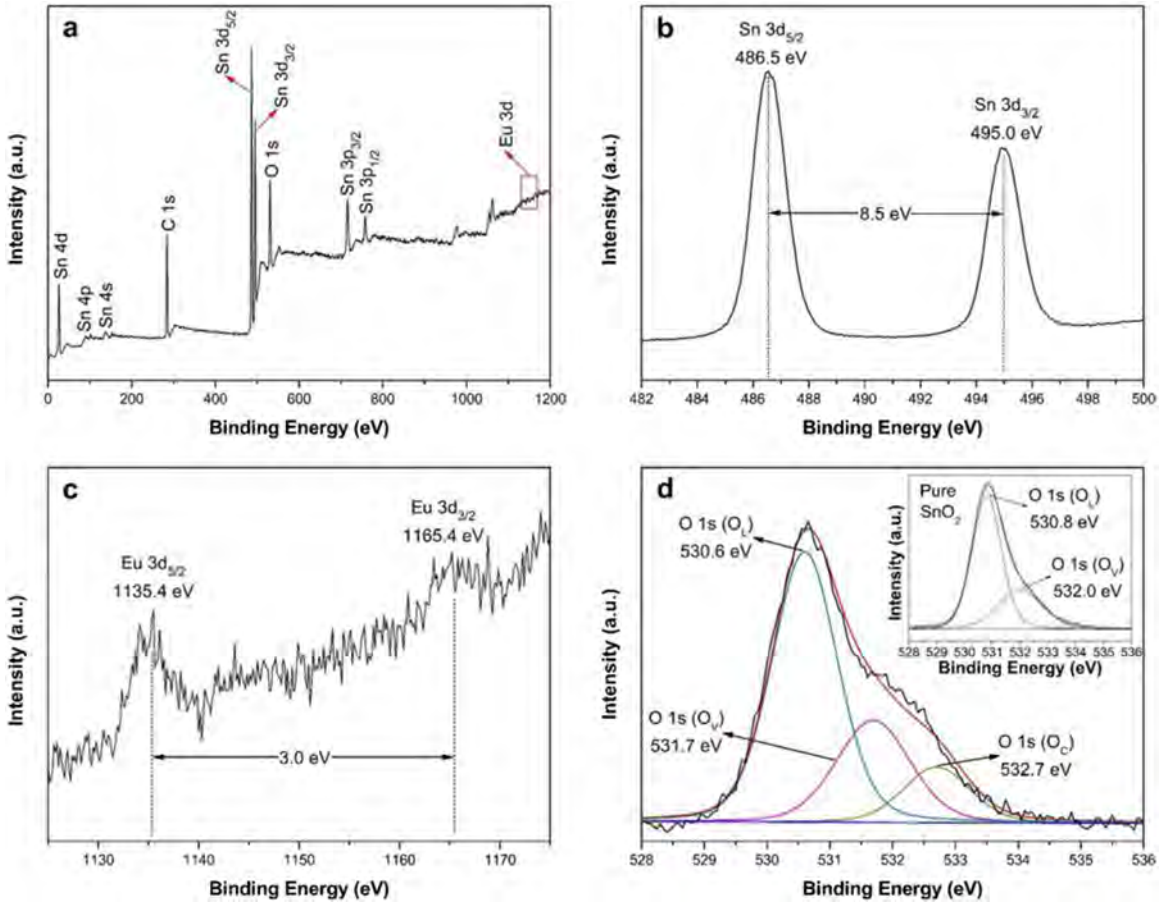

Fig. 4. XPS spectra of 2 mol% Eu-doped SnO_2 nanofibers, (a) survey spectrum and high-resolution spectra for (b) Sn3d, (c) Eu 3d and (d) O1s.

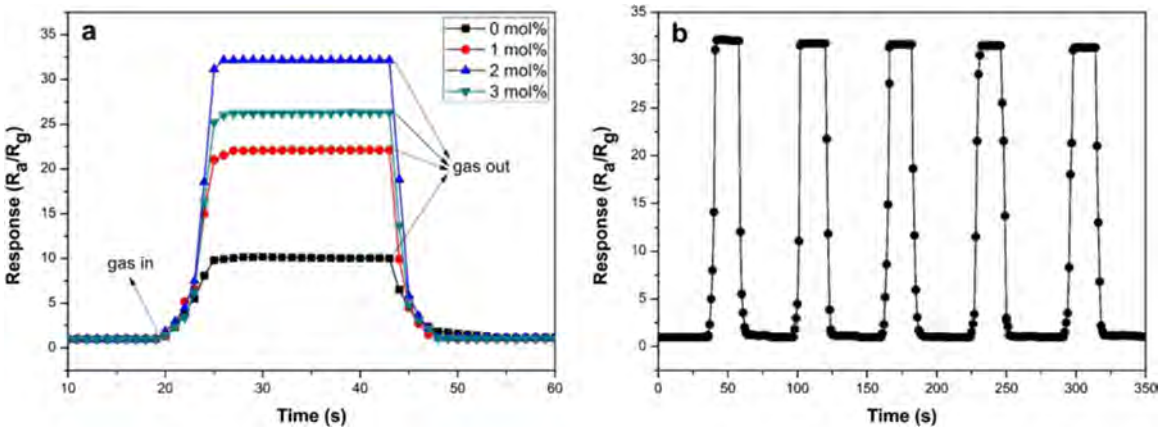

Fig. 6. (a) Dynamic response-recovery curves of pure and Eu-doped SnO_2 nanofibers against 100 ppm acetone. (b) Five periods of the response-recovery curve based on 2 mol% Eu-doped SnO_2 nanofibers.

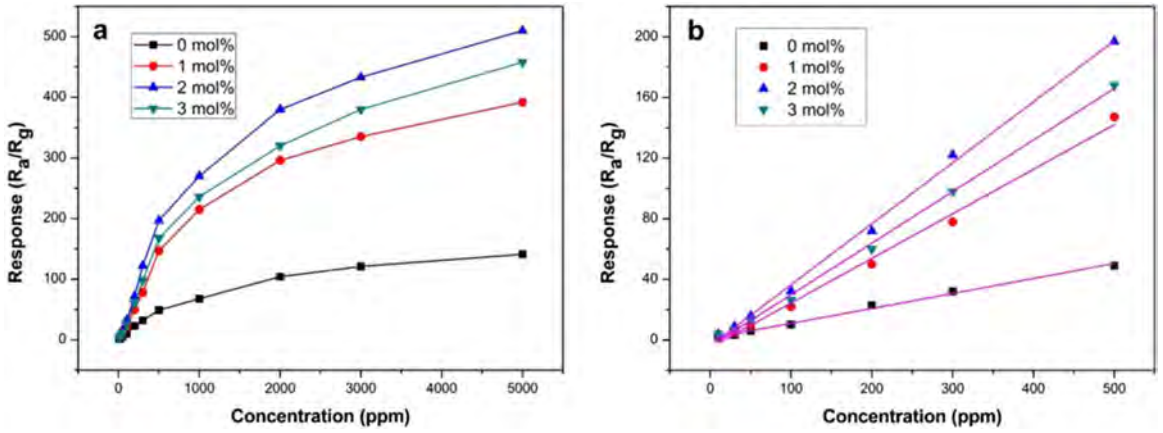

Fig. 7. (a) Responses of pure and Eu-doped SnO_2 nanofibers versus acetone concentration. (b) The calibration curves in the range of 10–500 ppm.

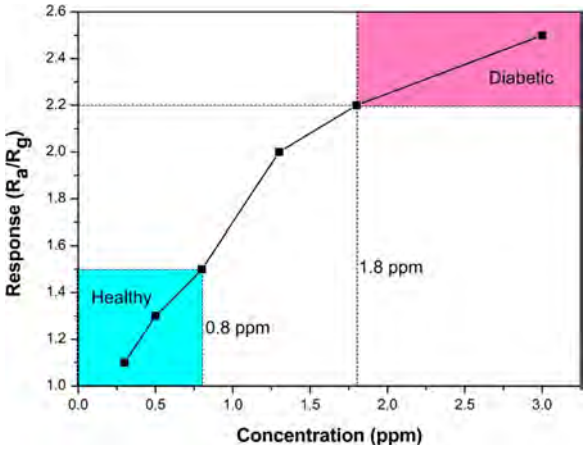

Fig. 8. Response of the 2 mol% Eu-doped SnO_2 sensor in sub-ppm concentrations.

found that the acetone response of the optimal sensor is below 1.5 for healthy humans (< 0.8 ppm) and above 2.2 for diabetic patients (> 1.8 ppm). This 46.7% response increase may allow the reliable diagnosis of diabetes by analyzing breath acetone.

The cross-selectivity is also an important parameter to evaluate the gas-sensing properties. Fig. 9(a) displays the responses of pure and Eu-doped SnO_2 nanofibers to 100 ppm of six gases, including acetone, ethanol, methanol, acetic acid, DMF and ammonia. It is noticed that the sensors based on Eu-doped SnO_2 nanofibers, especially the 2 mol% Eu-doped SnO_2 sensor, possess a much higher response to acetone than other gases compared with the pure SnO_2 sensor. The results reveal that the sensor based on 2 mol% Eu-doped SnO_2 nanofibers has an excellent discriminative ability to acetone. To research the long-time stability of fabricated sensors, the responses against 100 ppm acetone at 280 °C were repeatedly measured every 10 days. As shown in Fig. 9(b), all the sensors exhibit nearly constant signals in 60 days, implying the superior stability of these sensors.

3.4. Gas-sensing mechanism

In general, the gas-sensing mechanism of n-type semiconducting metal oxides is based on the change in resistance, which is caused by the absorption and desorption of oxygen molecules on the surface of metal oxides [43]. When Eu-doped SnO_2 nanofibers are exposed to air, oxygen molecules are absorbed on the surface of nanofibers, capturing electrons from the conduction band of SnO_2 to form chemisorbed oxygen species. An electron depletion layer will be generated on the surface during this process, leading to an increase of resistance. The formation of chemisorbed oxygen species can be described as follows:

$$O_2 \rightarrow O_2(ads) \quad (2)$$

$$O_2(ads) + e^- \rightarrow O_2^-(ads) \quad (3)$$

$$O_2^-(ads) + e^- \rightarrow 2O^-(ads) \quad (4)$$

$$O^-(ads) + e^- \rightarrow O^{2-}(ads) \quad (5)$$

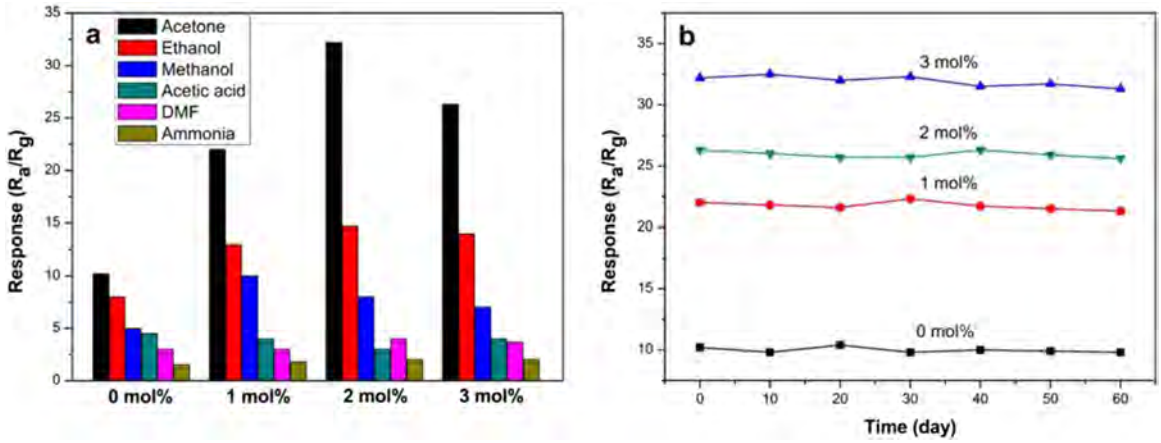

Fig. 9. (a) Responses of pure and Eu-doped SnO_2 nanofibers to 100 ppm of acetone, ethanol, methanol, acetic acid, DMF and ammonia. (b) Stability measurement of pure and Eu-doped SnO_2 nanofibers.

When the nanofibers are exposed to acetone, the ionized oxygen species will react with acetone molecules and release electrons back to the conduction band. These released electrons increase the electron concentration and result in a decreased resistance. The reactions can be described by the following equations [44,45]:

$$CH_3COCH_3(gas) + O^- \rightarrow CH_3COC^+H_2 + OH^- + e^- \quad (6)$$

$$CH_3COCH_3(gas) + OH^- \rightarrow CH_3CHO + CH_3O^- \quad (7)$$

$$CH_3CHO + O(bulk) \rightarrow CH_3COOH + O(vacancies) \quad (8)$$

$$CH_3COCH_3(gas) + O^- \rightarrow CH_3C^+O + CH_3O^- + e^- \quad (9)$$

$$CH_3C^+O \rightarrow C^+H_3 + CO \quad (10)$$

$$CO + O^{2-} \rightarrow CO_2 + 2e^- \quad (11)$$

According to the above mechanism, it can be concluded that the specific surface area of gas-sensing materials plays an important role in the enhancement of response. The high length-to-diameter ratio and net-like structure of 1D SnO_2 nanofibers can enhance the absorption of target gas molecules, leading to a high response value [46].

The improved acetone-sensing performance of Eu-doped SnO_2 nanofibers is mainly attributed to the increase of absorbed oxygen species. When Eu^{3+} ions diffuse into the SnO_2 lattice and substitute Sn^{4+} ions, the mismatch in ionic radius between Eu^{3+} (0.947 Å) and Sn^{4+} (0.69 Å) will result in the lattice distortion and defects. Oxygen vacancies are generated during the release of lattice distortion energy, and this process can be represented by the Kröger-Vink notations [47,48]:

$$Eu_2O_3 + 2e' \rightarrow 2Eu'_{Sn} + 3O^x_O + V^x_O \quad (12)$$

$$O_2 + 2V^x_O \rightarrow 2O^x_O + 4h \quad (13)$$

To restore the stoichiometry of metal oxides, oxygen vacancies will absorb atmospheric oxygen. It has been reported that the adsorption energy of target gas on the oxygen-vacancy site is 3 times larger than that on the perfect site [49]. That means the oxygen vacancies on the surface of SnO_2 can act as electron donors, which is very helpful to adsorbing oxygen molecules. Consequently, a large number of electrons are captured in air and released in acetone atmosphere, leading to a higher response. Moreover, the substitution of Sn^{4+} by Eu^{3+} will induce holes, resulting in a decrease in electron concentration [50]. Thus the resistance of SnO_2 nanofibers increase by Eu doping. In our experiments, the resistance of SnO_2 sensor is increased from 346 kΩ to 1.02 MΩ after adding 2 mol% Eu, which will eventually contribute to the acetone-sensing improvement.

The catalytic activity of rare earth oxides is another considerable factor for the acetone-sensing enhancement. When Eu_2O_3, an alkalescent metal oxide, is introduced into the SnO_2 system, a basic surface can be constructed. According to Eq. (7), the basic surface can not only enhance the catalytic activity for the dehydrogenation of acetone gas to CH_3CHO, but also that for the consecutive oxidation of CH_3CHO to CO_2 [51]. That is to say, Eu_2O_3 can accelerate the reactions between acetone molecules and absorbed oxygen species to release electrons to the conduction band, resulting in a enhanced response. However, when the doping level is higher than 2 mol%, the response begin to decrease. This is because redundant Eu^{3+} will be expelled from the SnO_2 crystal and form many clusters such as Eu-Eu or Eu-O, reducing the electric transduction of SnO_2 nanofibers [52]. Furthermore, acetone molecules will be burned on Eu_2O_3 clusters and transform into CO_2 and H_2O without creating any electric signals [53,54], so 2 mol% is the optimal doping ratio.

4. Conclusions

In summary, Eu-doped SnO_2 nanofibers with different molar ratios have been synthesized by simple electrospinning and calcination procedure. In comparison with pure SnO_2 nanofibers, large response value (32.2 for 100 ppm), short response/recovery time (4 s/3 s for 100 ppm), low detection limit (0.3 ppm) and good selectivity were simultaneously observed for 2 mol% Eu-doped SnO_2 nanofibers at 280 °C when utilized for acetone sensing. These enhanced acetone-sensing properties are attributed to the increase of absorbed oxygen species achieved by Eu doping and catalytic activity of Eu_2O_3. The results obtained in this paper indicate that Eu-doped SnO_2 nanofibers are promising for high-performance acetone sensors.

Acknowledgements

The work was supported by the research grants from the National Nature Science Foundation of China (Grant nos. 21274052 and 21474043), Jilin Provincial Science and Technology Department Project (Grant nos. 20130206064GX), and Changchun City Science and Technology Department Project (Grant nos. 13KG32).

References

[1] X. Li, H. Zhang, C.H. Feng, Y.F. Sun, J. Ma, C. Wang, G.Y. Lu, Novel cage-like α-Fe_2O_3/SnO_2 composite nanofibers by electrospinning for rapid gas sensing properties, RSC Adv. 4 (2014) 27552–27555.

[2] L. Cheng, S.Y. Ma, X.B. Li, J. Luo, W.Q. Li, F.M. Li, Y.Z. Mao, T.T. Wang, Y.F. Li, Highly sensitive acetone sensors based on Y-doped SnO_2 prismatic hollow nanofibers synthesized by electrospinning, Sens. Actuators B Chem. 200 (2014) 181–190.

[3] X.B. Li, S.Y. Ma, F.M. Li, Y. Chen, Q.Q. Zhang, X.H. Yang, C.Y. Wang, J. Zhu, Porous spheres-like ZnO nanostructure as sensitive gas sensors for acetone detection, Mater. Lett. 100 (2013) 119–123.

[4] L. Wang, A. Teleki, S.E. Pratsinis, P.I. Gouma, Ferroelectric WO_3 nanoparticles for acetone selective detection, Chem. Mater. 20 (2008) 4794–4796.

[5] Q.Q. Jia, H.M. Ji, P. Gao, X. Bai, Z.G. Jin, Control of the acetone sensitive and selective properties of WO_3 nanofibers by doping Co ions: effect of crystal symmetric structure on the responsivity of gas-solid boundaries for gas sensor, J. Mater. Sci. Mater. Electron. 26 (2015) 5792–5802.

[6] T. Thensil, S. Anandhan, Structure-property relationship of sol-gel electrospun ZnO nanofibers developed for ammonia gas sensing, J. Colloid Interface Sci. 432 (2014) 285–296.

[7] S. Wang, B. Xiao, T. Yang, P. Wang, C. Xiao, Z. Li, R. Zhao, M. Zhang, Enhanced HCHO gas sensing properties by Ag-loaded sunflower-like In_2O_3 hierarchical nanostructures, J. Mater. Chem. A 2 (2014) 6598–6604.

[8] D.Z. Wang, W.J. Zhou, P.G. Hu, Y. Guan, L.M. Chen, J.H. Li, G.C. Wang, H. Liu, J. Y. Wang, G.Z. Cao, H.D. Jiang, High Ethanol Sensitivity of Palladium/TiO_2 nanobelt surface heterostructures dominated by enlarged surface area and nano-Schottky junctions, J. Colloid Interface Sci. 388 (2012) 144–150.

[9] M. Righettoni, A. Tricoli, S.E. Pratsinis, Si: WO_3 sensors for highly selective detection of acetone for easy diagnosis of diabetes by breath analysis, Anal. Chem. 82 (2010) 3581–3587.

[10] C.H. Feng, X. Li, C. Wang, Y.F. Sun, J. Zheng, G.Y. Lu, Facile synthesis benzene sensor based on V_2O_5-doped SnO_2 nanofibers, RSC Adv. 4 (2014) 47549–47555.

[11] Z.J. Wang, Z.Y. Li, T.T. Jiang, X.R. Xu, C. Wang, Ultrasensitive hydrogen sensor based on Pd^0-loaded SnO_2 electrospun nanofibers at room temperature, ACS Appl. Mater. Interfaces 5 (2013) 2013–2021.

[12] T.T. Wang, S.Y. Ma, L. Cheng, J. Luo, X.H. Jiang, W.X. Jin, Preparation of Yb-doped SnO_2 hollow nanofibers with an enhanced ethanol-gas sensing performance by electrospinning, Sens. Actuators B Chem. 216 (2015) 212–220.

[13] D. Hu, B.Q. Han, S. Deng, Z.P. Feng, Y. Wang, J. Popovic, M. Nusko, Y. Wang, I. Djerdj, Novel mixed phase SnO_2 nanorods assembled with SnO_2 nanocrystals for enhancing gas-sensing performance toward isopropanol gas, J. Phys. Chem. C 118 (2014) 983–29840.

[14] T. Rakshit, S. Santra, I. Manna, S.K. Ray, Enhanced sensitivity and selectivity of brush-like SnO_2 nanowire/ZnO nanorod heterostructure based sensors for volatile organic compounds, RSC Adv. 4 (2014) 36749–36756.

[15] Y. Zeng, Y.Z. Wang, L. Qiao, Y.F. Bing, B. Zou, W.T. Zheng, Synthesis and the improved sensing properties of hierarchical SnO_2 hollow nanosheets with mesoporous and multilayered interiors, Sens. Actuators B Chem. 222 (2016) 354–361.

[16] J.S. Jang, S.J. Kim, S.J. Choi, N.H. Kim, M. Hakim, A. Rothschild, I.D. Kim, Thin-walled SnO_2 nanotubes functionalized with Pt and Au catalysts via the protein templating route and their selective detection of acetone and hydrogen sulfide molecules, Nanoscale 7 (2015) 16417–16426.

[17] S.J. Choi, B.H. Jang, S.J. Lee, B.K. Min, A. Rothschild, I.D. Kim, Selective detection of acetone and hydrogen sulfide for the diagnosis of diabetes and halitosis using SnO_2 nanofibers functionalized with reduced graphene oxide nanosheets, ACS Appl. Mater. Interfaces 6 (2014) 2588–2597.

[18] D. Li, Y.N. Xia, Electrospinning of nanofibers: reinventing the wheel? Adv. Mater. 16 (2004) 1151–1170.

[19] L.P. Chikhale, J.Y. Patil, A.V. Rajgure, F.I. Shaikh, I.S. Mulla, S.S. Suryavanshi, Structural, morphological and gas sensing properties of undoped and Lanthanum doped nanocrystalline SnO_2, Ceram. Int. 40 (2014) 2179–2186.

[20] S. Habibzadeh, A.A. Khodadadi, Y. Mortazavi, CO and ethanol dual selective sensor of Sm_2O_3-doped SnO_2 nanoparticles synthesized by microwave-induced combustion, Sens. Actuators B Chem. 144 (2010) 131–138.

[21] W.F. Qin, L. Xu, J. Song, R.Q. Xing, H.W. Song, Highly enhanced gas sensing properties of porous SnO_2-CeO_2 composite nanofibers prepared by electrospinning, Sens. Actuators B Chem. 185 (2013) 231–237.

[22] J.S. Lu, X.A. Cao, C.Y. Pan, L.F. Yang, G.B. Lai, J.L. Chen, C.Q. Wu, Studies of the cataluminescence of benzene homologues on nanosized γ-Al_2O_3/Eu_2O_3 and the development of a gas sensor for benzene homologue vapors, Sensors 6 (2006) 1827–1836.

[23] Y.S. Tan, Z.B. Fang, W. Chen, P.M. He, Structural, optical and magnetic properties of Eu-doped ZnO films, J. Alloy. Compd. 509 (2011) 6321–6324.

[24] K.C. Wang, B.J. Zhao, L. Gao, X-ray photoemission spectroscopy investigation of $CaTiO_3$: Eu for luminescence property: effect of Eu^{3+} ion, Mater. Res. Bull. 78 (2016) 31–35.

[25] P. Sun, X. Zhou, C. Wang, B. Wang, X.M. Xu, G.Y. Lu, One-step synthesis and gas sensing properties of hierarchical Cd-doped SnO_2 nanostructures, Sens. Actuators B Chem. 190 (2014) 32–39.

[26] R.Q. Xing, L. Xu, Y.S. Zhu, J. Song, W.F. Qin, Q.L. Dai, D.L. Liu, H.W. Song, Three-dimensional ordered SnO_2 inverse opals for superior formaldehyde gas sensing performance, Sens. Actuators B Chem. 188 (2013) 235–241.

[27] R.P.A. Hartman, D.J. Brunner, D.M.A. Camelot, J.C.M. Marijnissen, B. Scarlett, Electrohydrodynamic atomization in the cone-jet mode physical modeling of the liquid cone and jet, J. Aerosol Sci. 30 (1999) 823–849.

[28] A.P. Maciel, P.N. Lisboa-Filho, E.R. Leite, C.O. Paiva-Santos, W.H. Schreiner, Y. Maniette, E. Longo, Microstructural and morphological analysis of pure and Ce-doped tin dioxide nanoparticles, J. Eur. Ceram. Soc. 23 (2003) 707–713.

[29] Z.Y. Li, X.G. Wang, T. Lin, Highly sensitive SnO_2 nanofiber chemiresistors with a low optimal operating temperature: synergistic effect of Cu^{2+}/Au co-doping, J. Mater. Chem. A 2 (2014) 13655–13660.

[30] X.R. Xu, J.H. Sun, H.N. Zhang, Z.J. Wang, B. Dong, T.T. Jiang, W. Wang, Z.Y. Li, C. Wang, Effects of Al doping on SnO_2 nanofibers in Hydrogen Sensor, Sens. Actuators B Chem. 160 (2011) 858–863.

[31] Y.G. Zheng, J. Wang, P.J. Yao, Formaldehyde sensing properties of electrospun NiO-doped SnO_2 nanofibers, Sens. Actuators B Chem. 156 (2011) 723–730.

[32] T.K. Jia, J. Chen, Z. Deng, F. Fu, J.W. Zhao, X.F. Wang, F. Long, Facile synthesis of Zn-doped SnO_2 dendrite-built hierarchical cube-like architectures and their application in lithium storage, Mater. Sci. Eng. B 189 (2014) 32–37.

[33] Y. Uwamino, T. Ishizuka, H. Yamatera, X-ray photoelectron spectroscopy of rare earth compounds, J. Electron Spectrosc. Relat. Phenom. 34 (1984) 67–78.

[34] X. Yang, L.L. Xu, X.D. Yu, W. Li, K.X. Li, M.X. Huo, Y.H. Guo, Enhanced photocatalytic activity of Eu_2O_3/Ta_2O_5 mixed oxides on degradation of rhodamine B and 4-nitrophenol, Colloids Surf. A Physicochem. Eng. Asp. 320 (2008) 61–67.

[35] M.S. Yao, F. Ding, Y.B. Cao, P. Hu, J.M. Fan, C. Lu, F.L. Yuan, C.Y. Shi, Y.F. Chen, Sn doped ZnO layered porous nanocrystals with hierarchical structures and modified surfaces for gas sensors, Sens. Actuators B Chem. 201 (2014) 255–265.

[36] X.G. Han, H.Z. He, Q. Kuang, X. Zhou, X.H. Zhang, T. Xu, Z.X. Xie, L.S. Zheng, Controlling morphologies and tuning the related properties of nano/microstructured ZnO crystallites, J. Phys. Chem. C 113 (2009) 584–589.

[37] L.X. Zhang, J.H. Zhao, H.Q. Lu, L.M. Gong, L. Li, J.F. Zheng, H. Li, Z.P. Zhu, High sensitive and selective formaldehyde sensors based on nanoparticle-assembled ZnO micro-octahedrons synthesized by homogeneous precipitation method, Sens. Actuators B Chem. 160 (2011) 364–370.

[38] N. Yamazoe, J. Fuchigami, M. Kishikawa, T. Seiyama, Interactions of tin oxide surface with O, H_2O and H_2, Surf. Sci. 86 (1979) 335–344.

[39] M. Ghasdi, H. Alamdari, CO sensitive nanocrystalline $LaCoO_3$ perovskite sensor prepared by high energy ball milling, Sens. Actuators B Chem. 148 (2010) 478–485.

[40] J. Liu, W.B. Guo, F.D. Qu, C.H. Feng, C. Li, L.H. Zhu, J.R. Zhou, S.P. Ruan, W. Y. Chen, V-doped In_2O_3 nanofibers for H_2S detection at low temperature, Ceram. Int. 40 (2014) 6685–6689.

[41] E. Wongrat, P. Pimpang, S. Choopun, Comparative study of ethanol sensor based on gold nanoparticles: ZnO nanostructure and gold: ZnO nanostructure, Appl. Surf. Sci. 256 (2009) 968–971.

[42] M. Arienzo, L. Armelao, C.M. Mari, S. Polizzi, R. Ruffo, R. Scotti, F. Morazzoni, Macroporous WO_3 thin films active in NH_3 sensing: role of the hosted Cr isolated centers and Pt nanoclusters, J. Am. Chem. Soc. 133 (2011) 5296–5304.

[43] P. Sun, Y.X. Cai, S.S. Du, X.M. Xu, L. You, J. Ma, F.M. Liu, X.S. Liang, Y.F. Sun, G. Y. Lu, Hierarchical α-Fe_2O_3/SnO_2 semiconductor composites: hydrothermal synthesis and gas sensing properties, Sens. Actuators B Chem. 182 (2013) 336–343.

[44] X. Chi, C.B. Liu, L. Liu, Y. Li, Z.J. Wang, X.Q. Bo, L.L. Liu, C. Su, Tungsten trioxide nanotubes with high sensitive and selective properties to acetone, Sens. Actuators B Chem. 194 (2014) 33–37.

[45] X.L. Xu, Y. Chen, S.Y. Ma, W.Q. Li, Y.Z. Mao, Excellent acetone sensor of La-doped ZnO nanofibers with unique bead-like structures, Sens. Actuators B Chem. 213 (2015) 222–233.

[46] Y. Zhang, J.P. Li, G.M. An, X.L. He, Highly porous SnO_2 fibers by electrospinning and oxygen plasma etching and its ethanol-sensing properties, Sens. Actuators B Chem. 144 (2010) 43–48.

[47] P. Mohanapriya, H. Segawa, K. Watanabe, K. Watanabe, S. Samitsu, T.S. Natarajan, N. Victor Jaya, N. Ohashi, Enhanced ethanol-gas sensing performance of Ce-doped SnO_2 hollow nanofibers prepared by electrospinning, Sens. Actuators B Chem. 188 (2013) 872–878.

[48] W.Q. Li, S.Y. Ma, Y.F. Li, G.J. Yang, Y.Z. Mao, J. Luo, D.J. Gengzang, X.L. Xu, S. H. Yan, Enhanced ethanol sensing performance of hollow ZnO-SnO_2 core-shell nanofibers, Sens. Actuators B Chem. 211 (2015) 392–402.

[49] W. An, X. Wu, X.C. Zeng, Adsorption of O_2, H_2, CO, NH_3, and NO_2 on ZnO nanotube: a density functional theory study, J. Phys. Chem. C 112 (2008) 5747–5755.

[50] J.J. Wu, Q.W. Huang, D.W. Zeng, S.P. Zhang, L. Yang, D.S. Xia, Z.D. Xiong, C.S. Xie, Al-doping induced formation of oxygen-vacancy for enhancing gas-sensing properties of SnO_2 NTs by electrospinning, Sens. Actuators B Chem. 198 (2014) 62–69.

[51] T. Jinkawa, G. Sakai, J. Tamaki, N. Miura, N. Yamazoe, Relationship between ethanol gas sensitivity and surface catalytic property of tin oxide sensors modified with acidic or basic oxides, J. Mol. Catal. A Chem. 155 (2000) 193–200.

[52] J.P. Cheng, B.B. Wang, M.Z. Zhao, F. Liu, X.B. Zhang, Nickel-doped tin oxide hollow nanofibers prepared by electrospinning for acetone sensing, Sens. Actuators B Chem. 190 (2014) 78–85.

[53] L. Liu, Y. Zhang, G.G. Wang, S.C. Li, L.Y. Wang, Y. Han, X.X. Jiang, A.G. Wei, High toluene sensing properties of NiO-SnO_2 composite nanofiber sensors operating at 330 °C, Sens. Actuators B Chem. 160 (2011) 448–454.

[54] J.C. Belmonte, J. Manzano, J. Arbiol, A. Cirera, J. Puigorbe, A. Vila, N. Sabate, I. Cracia, C. Cane, J.R. Morante, Micromachined twin gas sensor for CO and O_2 quantification based on catalytically modified nano-SnO_2, Sens. Actuators B Chem. 114 (2006) 881–892.